Simulation of atmospheric transport and droplet–thin film collisions in desorption electrospray ionization†

Anthony B. Costa and R. Graham Cooks*

Received (in Cambridge, UK) 10th July 2007, Accepted 6th August 2007
First published as an Advance Article on the web 13th August 2007
DOI: 10.1039/b710511h

Computational fluid dynamics is used to model atmospheric transport and droplet–thin film (surface) collisions in desorption electrospray ionization; experimentally obtained droplet properties are replicated in the simulations while a "droplet pick-up" mechanism of analyte transport is confirmed.

Desorption electrospray ionization (DESI) is an ambient ionization method[1–4] used in mass spectrometry for chemical analysis of solid analytes at surfaces in the open atmosphere; it is finding a wide variety of applications.[5,6] Characteristics of the spray both before and after surface impact have been investigated by phase doppler anemometry (PDA).[7] These experiments indicate average droplet sizes of 2–4 μm and velocities between 100–200 m s^{-1} at 2 mm from the spray source. After surface collisions, small fast droplets tend to emerge closer to the surface, whereas larger droplets are found at larger angles. However, a fundamental understanding of the transport and collision processes is far from complete. Simulation of the DESI process is desired especially as the number and diversity of applications increase.[8–13] It is clear that certain combinations of substrate, spray and analyte are highly favored for DESI analysis. A non-empirical understanding of the system is therefore highly desirable. Previous work on the simulation of ionization mechanisms in mass spectrometry has focused on molecular modeling approaches to secondary ion mass spectrometry (SIMS) and matrix-assisted laser-desorption ionization (MALDI) mass spectrometry.[14–16] These molecular dynamics methods are not readily applied to the simulation of macroscopic, bulk fluid flow and particle transport regimes encountered in the DESI process at atmospheric pressure. Here, continuum transport theory is more appropriate and finite volume computational fluid dynamics (CFD) is adopted as a simulation methodology.

Two basic simulations are reported here: simulation of the spray transport due to fluid motion and a simulation of the droplet–surface impact. The first includes bulk fluid transport originating from the nebulizing gas at the DESI spray source and the motion of droplets after their collisions with the substrate surface. A three-dimensional mesh representative of a typical geometry of the DESI ionization source is generated using the open-source mesh generation utility *Gmsh*.[17] Three-dimensional elements of the mesh are generated using the Delaunay triangulation algorithm included in *Gmsh*. The inner capillary of the sprayer has an inner diameter of 100 μm and an outer diameter of 190 μm. The outer capillary has an inner diameter of 250 μm. The sprayer is positioned 2 mm from the substrate surface at an incident angle of 55° to the horizontal. The mesh is imported into the open-source continuum mechanics package *OpenFOAM*.[18,19] The influence of the reduced-pressure transport originating at the inlet of the mass spectrometer is neglected. This is done in order to probe only the evolution of the spray itself and to simplify subsequent data analysis, though it is recognized that inlet capillary transport will affect droplet evolution. The initial nebulizing gas velocity is set at 300 m s^{-1}. Droplet transport subject to the fluid environment is treated using a Stokes/Lagrangian droplet tracking mechanism previously implemented in *OpenFOAM*. The distribution of droplet sizes is approximated using a Rossin–Rammler distribution with mean diameter 3 μm and maximum and minimum sizes of 6.0 and 0.5 μm, respectively. Droplets are placed at the exit of the inner capillary of the spray source with an initial velocity of 180 m s^{-1} and an inner cone angle of 20°. There is a lack of understanding on the primary atomization mechanisms which drive droplet formation, but it is assumed that once droplets are formed they have some significant velocity magnitudes. All initial numerical values are derived from the phase doppler anemometry experiments. Collisions with the substrate surface are treated as fully elastic. Forces on droplets due to electrostatics, including droplet–droplet and droplet–field effects, are neglected. This has important implications which are discussed further in the description of results.

A representative image of the spray simulation is shown in Fig. 1. In the figure, droplets are represented as black spheres, each

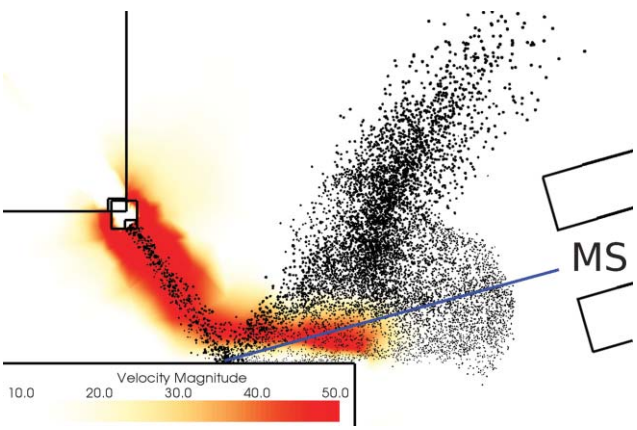

Fig. 1 Spray and fluid velocity illustration. Droplets are black spheres eight times their actual size. Background color indicates velocity magnitude of surrounding fluid. The blue line shows the optimum collection angle from experiments (~10°).

Department of Chemistry, Purdue University, West Lafayette, IN, USA. E-mail: cooks@purdue.edu; Fax: 765-494-9421; Tel: 765-494-5263
† Electronic supplementary information (ESI) available: Description of meshes, boundary conditions and computational procedures used in these simulations. See DOI: 10.1039/b710511h

of which is eight times the actual size of the droplet used in the simulation. The background color scheme indicates the velocity magnitude of the surrounding fluid. A number of interesting features are present in the simulation. It is clear from the data that the nebulizing gas originating at the sprayer flattens, or "hugs" the surface. Therefore the highest velocity and most significant fluid flow in the simulation occur at or very near the substrate boundary. This is shown in the figure as the red region near the surface itself.

This fluid motion drives two major modes of droplet motion after collisions with the surface. The first, a low altitude group, is comprised mainly of the smallest and fastest droplets in the simulation. These droplets are driven across the surface by the fluid flow, and equilibrate to the velocity of the surrounding fluid environment quickly due to their small size and therefore reduced momentum. The second group, a high altitude group, is made up mainly of larger droplets which, due to their greater momentum, are able to escape the influence of the sheath gas flow near the surface and continue in a direction closer to their specular reflection. These data agree extremely well with previous size and velocity distribution data collected from experimental work, where it was postulated that this effect was due primarily to the fluid environment.[7] This work supports that speculation. The experimental size and velocity distributions are shown in Table 1 as a function of height and distance from the primary spray impact region. As droplets move away from the surface in the low altitude group, a steady increase is seen in the velocities measured at 0.5 mm from the surface. Equivalently, droplets at greater distances from the surface do not show any significant velocities. The size distribution of droplets seems to exhibit the same behavior seen from the simulation: large droplets are seen further from the surface than small droplets.

It should be re-emphasized that this simulation includes no electrostatic forces. This has some interesting implications in that the salient features of the spray characteristics known from experiments are replicated without the inclusion of electrostatics. This makes sense given the high flow rates present in a DESI experiment. The inclusion of droplet–droplet electrostatic interactions in the model may widen the spray region, though this effect is likely minimal. Furthermore, the small, high velocity droplet group driven by the fluid flow close to the surface has a "takeoff" angle of approximately 10°. It has been shown that for most experimental systems the highest ion signal is obtained when the inlet of the mass spectrometer is positioned at a 10° angle to the surface when the incident spray angle is between 55–75°.[4] Even under the crude assumption of 100% surface collision elasticity this spatially resolved behavior is reproduced. The choice of fully elastic collisions here is necessary. Droplet collisions with surfaces will yield new progeny droplets expelled from the surface at various velocities and angles. This phenomenon is described further in the description of droplet–surface impact simulations below. However, the Stokes/Lagrangian methodology chosen here for the simulation of atmospheric transport does not lend itself to the inclusion of these droplet–surface effects, and so they are neglected. Future work will include more complex treatments of droplet–surface effects in Lagrangian sprays, informed from droplet–surface impact simulations described next.

Table 1 Experimental droplet size (diameter in μm) and velocities (m s^{-1}) as a function of height and distance from primary spray impact region. Data are shown as size–velocity pairs

Height/distance (mm)	3	5	8	11
4	–/–	–/–	3.3/2.9	1.3/1.7
2	1.9/2.1	2.1/0.5	3/3.9	1.3/1.1
1	2/2.2	1.1/0.4	1.3/2.7	1/9.4
0.5	1.3/2.7	0.8/3.8	0.9/11.4	1.1/21.7

The second (droplet–surface impact) simulation focuses on the collision of single droplets with thin liquid films on the substrate surface. The impact of droplets with thin liquid films and dry, wettable substrates has been studied previously, though this is the first work specific to droplets and films characteristic of the DESI environment.[25] A structured, rectangular, two-dimensional mesh is created using the *blockMesh* utility included in *OpenFOAM*. Two-dimensional systems are used due to computational constraints. The system is defined to be composed of two fluids, air and water. Kinematic viscosity and density of the phases are defined in Table 2. A water film of 1 μm thickness is placed at the bottom of the simulation region and a 3 μm water droplet is set in motion at 120 m s^{-1} and a 55° incident angle to the surface. Three phases are tracked independently: the droplet, surface and air. In this way it is possible to analyze the origins of various components of droplets leaving the surface after a collision. The surface tension between the water droplet and the thin water film is defined as zero. The results of a droplet–surface collision are visualized by drawing contours of the air–liquid boundary at time $t = 4.5$ μs to optimize the depiction of the droplets.

A number of features are immediately apparent from the visualization of progeny droplet production after the droplet–thin film collision. The total liquid, Fig. 2, shows the production of a larger number of high velocity droplets exiting the surface. These droplets have velocities ranging from the incident droplet velocity of 120 m s^{-1} to 0 m s^{-1} by the time the simulation is completed (not shown). The first droplets leave the surface with the highest velocity at a small angle to the surface. This simulation shows a "jetting" effect after the collision, in which a series of small droplets (on the order of 1 μm in diameter) are ejected from the surface. The size of these droplets leaving the surface agrees with previously published experimental work on droplet size profiles after surface collisions.[7] Further, the takeoff angle of the progeny droplets ranges from 0 to 15°.

When tracking the surface liquid and impacting droplet liquid separately, we find that droplets leaving the surface are comprised of liquid originating from the substrate surface as well as liquid originating from the incident droplet. This result lends evidence to the possibility of a two-step analyte pickup mechanism in DESI, whereby an initial surface film consisting of solvent and analyte is laid down by the sprayer, the analyte of interest being contained within the wetted surface. This "droplet pick-up" mechanism occurs as an incident droplet collision desorbs surface liquid and transports it into the mass spectrometer.

Table 2 Kinematic viscosity and density for each phase in the droplet impact simulation

Phase	Kinematic viscosity (m^2 s^{-1})	Density (kg m^{-3})
water	1.0×10^{-6}	1.0×10^{3}
air	1.48×10^{-5}	1.0

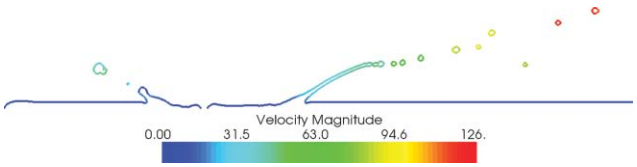

Fig. 2 Contours of liquid occupation at $t = 4.5$ μs after droplet–surface collision. Note the "jetting" phenomenon yielding high velocity low-angle forward-scattered micro-droplets and the presence of low-velocity back-scattered droplets.

It has been suggested in recent work that the existence of a thin film or wetted substrate is evidenced by a delay in achieving maximum ion intensity seen as a DESI experiment is begun.[12] The structure and properties of such a film are certainly substrate dependent and may vary significantly depending on the experimental configuration.

This mechanism is especially interesting when considering the chemistry that might be occurring during the course of a DESI experiment. Recent work has shown enhanced selectivity and sensitivity by using a reactive DESI approach, where selective reactivity can be achieved by the choice of spray solvent. This has been shown in studies of enhanced explosives and pharmaceutical sample detection as well as functional group recognition in certain systems.[20–24] The current work sheds significant light on this mechanism, as reactivity in the solution phase, both in the wetted surface and in the progeny droplet taking off from the surface, may be involved.

The simple models in computational fluid dynamics used here are successful in describing many of the droplet characteristics observed in DESI experiments without the use of electrostatic simulations, suggesting droplet transport is driven primarily by the fluid environment. Further, droplet–thin film collisions replicate basic experimental knowledge on progeny droplet size and velocity distributions. A three-phase simulation indicates that analyte contained within a thin film may be picked up by a high velocity droplet collision. Work in progress focuses on the influence of droplet–thin film collision parameters. These include studies focusing on the influence of droplet size, velocity and angle as well as the thin film thickness. Simulations including compressible and turbulent flow into the mass spectrometer as well as electrostatic droplet–droplet and droplet–field interactions are forthcoming.

Jason Green and Andre Venter are gratefully acknowledged for helpful discussions during the course of this work.

This work was supported by funding from the Office of Naval Research (ONR) under grant No. N00014-05-1-0405.

Notes and references

1 C. N. McEwen, R. G. McKay and B. S. Larsen, *Anal. Chem.*, 2005, **77**, 7831.
2 R. B. Cody, J. A. Laramée and H. D. Durst, *Anal. Chem.*, 2005, **77**, 2297.
3 J. Shiea, M.-Z. Huang, H.-J. Hsu, C.-Y. Lee, C.-H. Yuan, I. Beech and J. Sunner, *Rapid Commun. Mass Spectrom.*, 2005, **19**, 3701.
4 Z. Takats, J. M. Wiseman and R. G. Cooks, *J. Mass Spectrom.*, 2005, **40**, 1261.
5 Z. Takats, J. M. Wiseman, B. Gologan and R. G. Cooks, *Science*, 2004, **306**, 471.
6 R. G. Cooks, Z. Ouyang, Z. Takats and J. M. Wiseman, *Science*, 2006, **311**, 1566.
7 A. Venter, P. E. Sojka and R. G. Cooks, *Anal. Chem.*, 2006, **78**, 8549.
8 J. P. Williams and J. H. Scrivens, *Rapid Commun. Mass Spectrom.*, 2005, **19**, 3643.
9 H. Chen, Z. Pan, N. Talaty, D. Raftery and R. G. Cooks, *Rapid Commun. Mass Spectrom.*, 2006, **20**, 1577.
10 H. Chen, Z. Pan, D. Raftery and R. G. Cooks, *Angew. Chem., Int. Ed.*, 2006, **45**, 7188.
11 Y. Song, N. Talaty, W. A. Tao, Z. Pan and R. G. Cooks, *Chem. Commun.*, 2007, 61.
12 M. S. Bereman and D. C. Muddiman, *J. Am. Soc. Mass Spectrom.*, 2007, **18**, 1093.
13 C. Ricci, L. Nyadong, F. M. Fernandez, P. N. Newton and S. G. Kazarian, *Anal. Bioanal. Chem.*, 2007, **387**, 551.
14 K. Liu, C. Yong, B. J. Garrison and J. Vickerman, *J. Phys. Chem. B*, 1999, **103**, 3195.
15 B. Arezki, A. Delcort, B. J. Garrison and P. Bertrand, *J. Phys. Chem. B*, 2006, **110**, 6832.
16 L. Zhigilei, E. Leveugle, B. Garrison, Y. Yingling and M. Zeifman, *Chem. Rev.*, 2003, **103**, 321.
17 http://www.geuz.org/gmsh/.
18 H. Weller, G. Tabor, H. Jasak and C. Fureby, *Comput. Phys.*, 1998, **12**, 620.
19 http://www.opencfd.co.uk/openfoam/.
20 H. Chen, I. Cotte-Rodriguez and R. G. Cooks, *Chem. Commun.*, 2006, 597.
21 H. Chen, N. Talaty, Z. Takats and R. G. Cooks, *Anal. Chem.*, 2005, **77**, 6915.
22 I. Cotte-Rodriguez, Z. Takats, N. Talaty, H. Chen and R. G. Cooks, *Anal. Chem.*, 2005, **77**, 6755.
23 M. Nefliu, R. G. Cooks and C. Moore, *J. Am. Soc. Mass Spectrom.*, 2006, **17**, 1091.
24 L. Nyadong, M. Green, V. De Jesus, P. Newton and F. Fernandez, *Anal. Chem.*, 2007, **79**, 2150.
25 I. V. Roisman and C. Tropea, *Int. J. Multiphase Flow*, 2005, **31**, 179.